# Characterization of Titanium Films Deposited with a Cathodic Arc Using a Straight Magnetic Duct

# Characterization of Titanium Films Deposited with a Cathodic Arc Using a Straight Magnetic Duct

**F. Bermeo [1,2], H. Della Torre[3], A. Kleiman[3*], F. Minotti[3†] , A. Márquez[3†‡]**

[1]Universidad Santiago de Cali, Calle 5 # 62-00, Cali, Colombia

[2]Universidad del Valle, Calle 13 # 100-00, Cali, Colombia

[3]Instituto de Física del Plasma, FCEN, Universidad de Buenos Aires – CONICET, Ciudad Universitaria, C1428EGA Buenos Aires, Argentina

E-mail: adriana@tinfip.lfp.uba.ar

**Abstract**. Nanostructured Ti films were obtained employing a cathodic arc with a straight magnetic filter. The films were characterized using X-ray diffraction, scanning electron and atomic force microscopy. The films were found to be dense and with columnar grains, whose size increased with the exposure time. The number of macroparticles, the film roughness and the deposition rate were also analyzed, and the latter compared with the results of a fluid plasma model. Number of macroparticles and film roughness in samples located ahead of the magnetic duct inlet were higher than those determined from samples placed inside the magnetic duct. The deposition rate depended on the axial and radial position inside the duct. The thickness along the radial position was more uniform for samples located at axial positions near the filter extremes, but the mean deposition rate was lower at these positions. Measured and modeled deposition rates agreed reasonably well.

## 1. Introduction

The application of cathodic arc devices to thin film growth has been widely investigated due to the plasma characteristics, mainly a high charge density and ions with high kinetic energy, which promote the formation of dense nanostructured films with good adhesion and a very high deposition rate [1].

In cathodic arc discharges a metallic plasma jet is ejected from the cathode surface [2]. If a substrate is located facing the plasma jet its surface is coated with a metallic film. The substrate conditions, temperature and bias with respect to the plasma potential used during the deposition process influence the structure, morphology and adhesion of the film. The main disadvantage of vacuum arc deposition is the emission of macroparticles (MPs) from the cathode. MPs in the coatings produce protuberances and depressions on the substrate surface that not only increase its roughness, but also degrade its mechanical properties. Employing a magnetic field parallel to the plasma jet, the ions are concentrated in this direction and the plasma density increases, so that the deposition rate increases and the fraction of MPs decreases. However, the use of magnetic fields leads to a loss of

[*] Fellow of the CONICET
[†] Member of the CONICET
[‡] Corresponding author

uniformity in the film thickness. Counting with a fluid model for the plasma, which allows to calculate the ion density as a function of the position inside the straight duct for different magnetic field values, helps to determine the best magnetic field value and axial position to obtain thickness uniformity adequate to the employed sample.

In this work titanium films deposited by a cathodic arc on stainless steel and silicon substrates with a straight magnetic duct were study. A two dimensional fluid model for the plasma flow through the magnetized duct was employed to fit the experimental behavior of the deposition rate as a function of the axial and radial positions. Values of the floating potential at the entrance of the filter were used as input for the model.

## 2. Experiment

The experiment was carried out in a d-c vacuum arc system, which is shown schematically in Figure 1. The discharge was produced between a cylindrical Ti cathode (60 mm in diameter) and a grounded annular Cu anode (80 mm in diameter). Both electrodes were mounted on an insulating piece that set an electrode separation of about 15 mm. The cathode was surrounded by a floating shield. The discharge circuit consisted in a current supply (18 kW, 150 A) in parallel with a capacitor bank (165 mF) connected to the electrodes through a series inductor (2.8 mH) in order to provide arc stability. A tungsten striker brought into contact with the cathode surface and later removed was employed to trigger the discharge. A stainless steel duct 25 cm long and 10 cm in diameter was connected electrically isolated behind the anode. A magnetic field was established by an external coil wrapped around the stainless steel tube. The solenoid beginning was located at 20 cm from the cathode surface. The arc current was 120 A. The magnetic field in the center of the solenoid was 120 G. The vacuum system, composed of a mechanical and two diffusion pumps, kept the pressure chamber at $10^{-5}$ mbar.

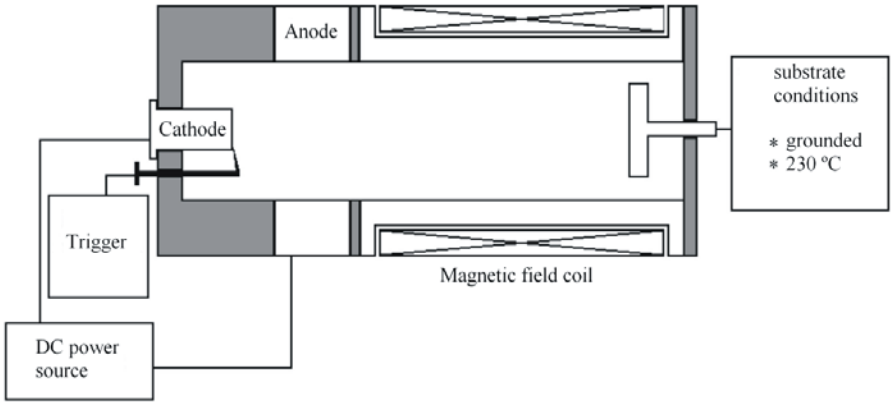


**Figure 1.** Schematic diagram of the d-c vacuum arc system.

The substrates were disks (19 mm in diameter and 2 mm in thickness) of stainless steel 316 and pieces of silicon (100) doped with Boron. They were placed at different axial distances from the cathode surface and mounted on a heater that holds the temperature at (210 ± 10) ºC. The exposure time to the discharge for growing the films was varied from 10 to 30 s.

The samples were weighted prior to and after the coating. From the measured deposited mass, the mean deposition rates were evaluated. The film thicknesses at different radial positions for the steel samples were determined by employing a Calotester. In this technique a hemispherical crater across the coating was eroded with a steel ball (30 mm in diameter) which was coated with a standard metallurgical diamond lapping paste and rotated during 2 min. The local deposition rates were estimated from the thickness. The film structure was analyzed by x-ray diffraction (XRD) with a

Philips PW 3710 diffractometer using *Cu*K$_\alpha$ radiation. It was operated with glancing angle geometry by using a Philips thin film attachment, with an angle of incidence of 1 deg.

The film surface was characterized. The morphology was studied by scanning electron microscopy (SEM) with a Philips ElectroScan 2010 microscope and by atomic force microscopy in tapping mode with a Nanoscope III Digital-VEECO.

Three probes located at different radial positions were employed to measure the floating potential along the filter. The probes were spherical Cu tips of diameter D = 3 mm with holders insulated from the plasma by double glass tubes. A high-impedance resistor was employed to register the floating potential of the collecting probes. The electrical signals were registered in a four channel digitizing oscilloscope (Tektronix 2014, sampling rate of 250 Ms/s, analogical bandwidth of 500 MHz).

## 3. Plasma model

We consider time independent, axially symmetric fluid equations for the plasma electrons and ions. At the low densities considered collisions between electron and ions will be neglected, and temperatures of each species taken as constant [3]. In this way, the momentum equation for the electrons, neglecting their inertia, is

$$T_e \nabla \ln n_e + e\left(-\nabla\varphi + \mathbf{u}_e \times \mathbf{B}\right) = 0, \tag{1}$$

with $e$ the elementary charge (absolute value), $T_e$ the electron temperature, $n_e$ the electron number density, $\mathbf{u}_e$ the electron fluid velocity, and $\varphi$ the electrostatic potential. This equation is projected along a magnetic field line to obtain $T_e \ln n_e - e\varphi = const$ for each magnetic line. The magnetic line which at $z = 0$ has coordinate $r = r_0$ has the representation $r_0 = r_0(r, z)$ so that one can write

$$T_e \ln n_e(r,z) - e\varphi(r,z) = T_e \ln n_e\left[r_0(r,z), 0\right] - e\varphi\left[r_0(r,z), 0\right]. \tag{2}$$

One can thus relate the electron density to the electrostatic potential. Also, by quasi-neutrality, the ion number density is $n_i = Zn_e$, with $Z$ the average ion charge state. In this way, the equation for the ion fluid velocity $\mathbf{u}$ is

$$m_i(\mathbf{u}\cdot\nabla)\mathbf{u} = -T_i \nabla \ln n_i + Ze\left(-\nabla\varphi + \mathbf{u}\times\mathbf{B}\right) - \lambda\mathbf{u}, \tag{3}$$

for ions of mass $m_i$ and temperature $T_i$. Here, $\lambda \approx m_i V_0^2/(c_s a)$ models ion-sound turbulent viscous effects ($a$ is the filter radius, $c_s$ is the ion sound velocity, and $V_0$ a characteristic ion velocity). The equation for $\varphi$, given the relation (2) and quasi-neutrality, can be obtained from the ion continuity equation,

$$\frac{1}{r}\frac{\partial}{\partial r}(r j_r) + \frac{\partial j_z}{\partial z} = 0, \tag{4}$$

where $j_z = n_i u_z$, and

$$j_r = n_i u_r - D_A \frac{\partial n_i}{\partial r}. \tag{5}$$

The last term in Eq. (5) accounts for radial ambipolar diffusion of ions, limited by electron Bohm diffusion across magnetic lines [4], so that

$$D_A = \left(Z + T_i/T_e\right)\frac{T_e}{16eB}. \tag{6}$$

In order to obtain a system of ordinary differential equations the following explicit *r* dependence is considered:

$$u_r(r,z)=K(z)r;\ u_\varphi(r,z)=\Omega(z)r;\ u_z(r,z)=V(z);\ \varphi(r,z)=A(z)\ \ r^2+C(z). \quad (7)$$

Replacement of expressions (7) in Eqs. (3)-(4), together with quasi-neutrality, after equating equal powers of *r*, result in a system of ordinary first order equations for $A(z)$, $C(z)$, $K(z)$, $\Omega(z)$, and $V(z)$ that can be solved by standard methods once the values of these functions are given at $z = 0$.

## 4. Results and discussion

Typical XRD spectra obtained from a coated sample is depicted in Figure 2. In the same picture, as reference, a XRD spectrum of the steel substrate and the 2θ-positions of the Bragg peaks corresponding to Ti are included.

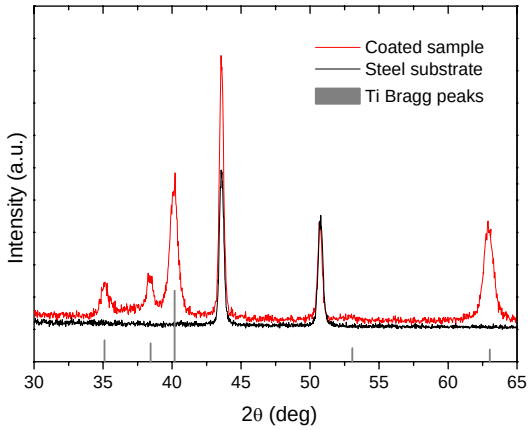


**Figure 2.** XRD patterns obtained from Ti deposited on stainless steel substrates.

Figure 3 shows typical SEM micrographs (magnification of 500x) of films obtained at different axial position and at an exposure time of 30s. Fig. 3 a) corresponds to a sample placed outside the magnetic duct, 5 cm before the solenoid beginning ($z = -5$ cm), being the position nearest the cathode. Fig. 3 b), c) and d) were taken from samples situated inside the duct at $z = 0$, 5 and 7.5 cm, respectively. Position $z = 0$ indicates the solenoid entrance and at $z = 7.5$ cm the magnetic field already reached the maxim value (120 G). It can be noted from the figures that the number and size of macroparticles decreased as the axial distance was increased. At $z = -5$ cm the largest macroparticle diameter was ~ 15 nm whereas at $z = 7.5$ cm was ~ 7 nm.

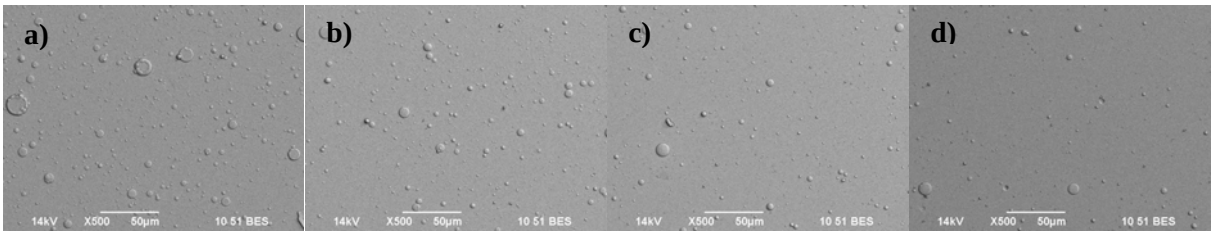


**Figure 3.** SEM micrographs of films obtained at different axial positions: a) $z = -5$ cm, b) $z = 0$, c) $z = 5$ cm, and d) $z = 7.5$ cm. Magnification of 500x.

The number of macroparticles also depended on the exposure time, the number increased as the time increased. AFM images acquired from films exposed to the discharge at 2 s and 20 s, on regions without the presence of macroparticles ($z = 7.5$ cm), display the surface morphologies shown in Figure

4. In both cases, the film surfaces are composed of columnar grains, pretty dense and without the presence of voids. From height profiles and roughness measurements registered on AFM images of films with different exposure time, the grain size and the roughness mean square were plotted as function of the exposure time in Figure 4 c). The columnar grain size increased as the time increased enlarging the surface roughness. The grain size varied from 2 nm to 55 nm for exposure time from 2 to 30 s, respectively.

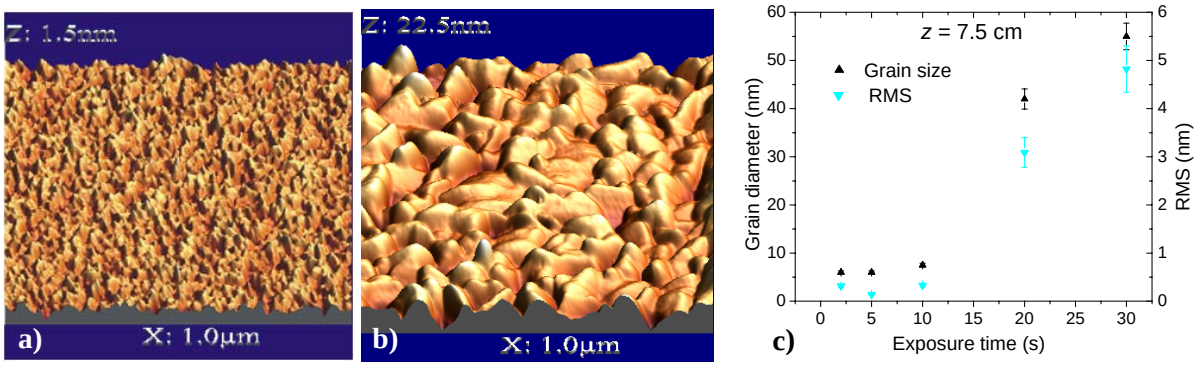


**Figure 4.** AFM images from films grown at $z$ = 7.5 cm with a) 2 s and b) 20 s exposure time. c) Film roughness and grain size as functions of the exposure time.

Mean deposition rate determined from the deposited mass weighting and the local deposition rates at the center, at 0.5 cm and at 1 cm off the center found from the thickness measurements are plotted in Figure 5. These results were obtained from samples exposed to the discharge during 120 s.

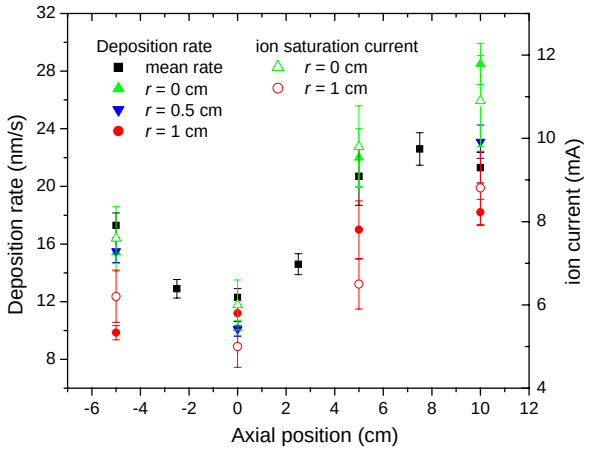


**Figure 5.** Deposition rate and ion current at different axial positions.

Since the ion energy loss can be neglected at the working pressure, the deposition can be taken proportional to the ion density. The deposition rate and the floating potential as function of $z$ for the different radial positions were compared with the output obtained from the 2D fluid model for the plasma in Figure 6. The floating potential measured outside the solenoid at $z$ = -5 cm was employed as input for the model. The deposition rate position inside the duct agreed reasonably well with the ion density profiles determined from the 2D fluid model for the plasma jet, and the potential profiles were reasonably fitted.

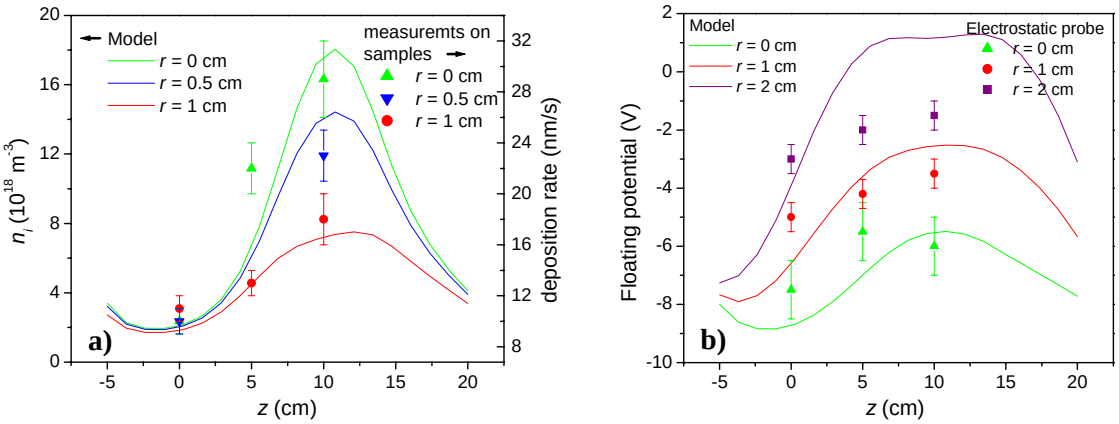


**Figure 6.** a) Modelled ion density (lines) and measured deposition rates (symbols). b) Modelled (lines) and measured (symbols) plasma potential.

## 5. Conclusions

Nanostructured Ti films were obtained employing a cathodic arc with a magnetic straight filter. The films were dense and with columnar grains, whose size increased with the exposure time from 5 to 50 nm for time ranging from 2 to 20 s, respectively. The number of macroparticles and the surface roughness in samples located ahead of the magnetic duct inlet were higher than those determined from samples placed inside the magnetic duct. The deposition rate depended on the axial and radial positions inside the duct. The thickness along the radial position was more uniform for samples located at axial positions near the filter extremes, but the mean deposition rate was lower at these positions.

The deposition rate as a function of the position inside the duct agreed reasonably with the ion density profiles determined from the 2D fluid model for the plasma jet, turning this model a useful tool to predict the radial profile of the coating.

## Acknowledgments

This work was supported by grants from Universidad de Buenos Aires, CONICET and MinCyT-Colciencias (CO/08/11). The authors would like to thank Diego G. Lamas for his collaboration in the XRD measurements at CINSO (CONICET-CITEDEF)

## References

[1] Vyskocil J and Musil J 1992 *J. Vac. Sci. Technol.* A **10** 1740
[2] Boxman RL, Sanders DM and Martin PJ (Eds.) 1995 *Handbook of Vacuum Arc Science and Technology, Fundamentals and Applications* (Park Ridge, NJ: Noyes)
[3] Giuliani L, Minotti F O, Grondona D and Kelly H 2007 *IEEE Trans. Plasma Sci*. **35** 1710
[4] Lieberman M and Lichtenberg A 2005 *Principles of Plasma Discharges and Material Processing* (Hoboken, NJ: Wiley-2nd Edition) pp 152-154